# Structure-Induced Enhancement in Electrooxidation of Trimetallic FePtAu Nanoparticles

Sen Zhang,[†,§] Shaojun Guo,[†,§] Huiyuan Zhu,[†] Dong Su,[‡] and Shouheng Sun*[,†]

[†]Department of Chemistry, Brown University, Providence, Rhode Island 02912, United States
[‡]Center for Functional Nanomaterials, Brookhaven National Laboratory, Upton, New York 11973, United States

**S** *Supporting Information*

**ABSTRACT:** Using FePtAu nanoparticles (NPs) as an example, this Communication demonstrates a new structure-control strategy to tune and optimize NP catalysis. The presence of Au in FePtAu facilitates FePt structure transformation from chemically disordered face-centered cubic (*fcc*) structure to chemically ordered face-centered tetragonal (*fct*) structure, and further promotes formic acid oxidation reaction (FAOR). The *fct*-FePtAu NPs have mass activity as high as 2809.9 mA/mg Pt and retain 92.5% of this activity after a 13 h stability test. They become the most efficient NP catalyst ever reported for FAOR. This structure-control strategy can be extended to other multimetallic NP systems, providing a general approach to advanced NP catalysts with desired activity and durability control for practical applications.

$\mathbf{R}$ecent advances in nanoparticle (NP) synthetic methodology have led to the formation of various monodisperse metallic NPs with ever-increasing activity to catalyze oxidation of fuel (hydrogen, formic acid, or alcohol) and reduction of oxygen in polymer electrolyte membrane fuel cell conditions.[1−3] Among all the NPs studied, Pt and its alloy NPs have constantly been the catalysts of choice due to their high activity for fuel oxidation and oxygen reduction reactions (ORR).[4−12] However, these Pt-based NPs have shown serious limitations in their fuel cell catalysis: they are unstable in the corrosive electrochemical environment and prone to deactivation by reaction intermediate species such as carbon monoxide.[13] As a result, NP catalysts based on elemental Pt and composition-controlled Pt-alloys are far from optimized for fuel cell applications. Very recently, core/shell-type NPs with a thin (<2 nm), uniform coating of Pt-shell were prepared and demonstrated to be a robust class of catalyst for ORR.[14−16] Despite this progress, there is still no reliable approach to NP catalysts with simultaneous enhancement in both activity and durability for practical fuel oxidation reactions.

This Communication presents a new structure-control strategy to tune and optimize NP catalysis for fuel oxidations. NPs, especially multimetallic NPs, can adopt different crystal structures. For example, as synthesized from a high-temperature solution-phase reaction, monodisperse binary FePt NPs have the chemically disordered face-centered cubic (*fcc*) structure, in which Fe and Pt atoms occupy randomly the *fcc* crystal lattice.[17] When further annealed, the *fcc* structure can be converted into the chemically ordered face-centered tetragonal (*fct*) structure,

in which Fe and Pt atoms form alternating atomic layers stacked along one specific direction.[17] Such a structure conversion in FePt can result in a drastic magnetic property change from superparamagnetism to ferromagnetism[18] and in chemical stability increase in acid solutions.[19] It is this chemical stability increase in *fct*-FePt that led to the current work to explore structure-induced NP catalysis for electrooxidation reactions with simultaneous enhancement in both activity and durability. The catalyst described here is monodisperse trimetallic FePtAu NPs. The presence of Au in FePtAu facilitates FePt structural transformation from *fcc* to *fct*, with Au segregating on the *fct*-FePt surface, and further promotes formic acid oxidation reaction (FAOR)—the anode reaction that is used to power direct formic acid fuel cells.[20] Compared to Pt and FePt NPs catalysts, the *fct*-FePtAu NPs show high CO poisoning-resistance, achieve mass activity of 2809.9 mA/mg Pt, and retain 92.5% of this activity after a 13 h stability test. They become the most active and durable catalyst ever reported for FAOR.

FePtAu NPs were synthesized by co-reduction of platinum acetylacetonate ($Pt(acac)_2$) and chloroauric acid hydrate ($HAuCl_4 \cdot xH_2O$) and thermal decomposition of iron pentacarbonyl ($Fe(CO)_5$) (Supporting Information). In the synthesis, excess $Fe(CO)_5$ was added to function both as a reducing agent and as a Fe precursor for its alloying with Pt and Au. Oleylamine and tetradecylphosphonic acid were used to stabilize the NPs. FePtAu compositions were controlled by varying the molar ratios of $Pt(acac)_2$, $HAuCl_4 \cdot xH_2O$, and $Fe(CO)_5$ and were analyzed by inductively coupled plasma—atomic emission spectroscopy (ICP-AES) (Table S1). Also, 4 nm $Fe_{55}Pt_{45}$ NPs were synthesized similarly without the presence of Au salt. Transmission electron microscopy (TEM) images show that the as-synthesized FePt and FePtAu NPs have an average size of 4 ± 0.2 nm for $Fe_{55}Pt_{45}$ (Figure S1), 4 ± 0.2 nm for $Fe_{42}Pt_{44}Au_{14}$ (Figure S2A), 4 ± 0.2 nm for $Fe_{43}Pt_{37}Au_{20}$ (Figure 1A), and 4 ± 0.3 nm for $Fe_{34}Pt_{34}Au_{32}$ NPs (Figure S2B).

FePt NPs are often synthesized by reduction of $Pt(acac)_2$ and thermal decomposition of $Fe(CO)_5$ in the presence of oleic acid and oleylamine.[17] This same recipe does not work for the current synthesis of FePtAu NPs with the desired size and Fe/Pt/Au composition controls. However, when oleic acid is replaced by tetradecylphosphonic acid, co-reduction of $Pt$-$(acac)_2$ and $HAuCl_4$ and decomposition of $Fe(CO)_5$ yield
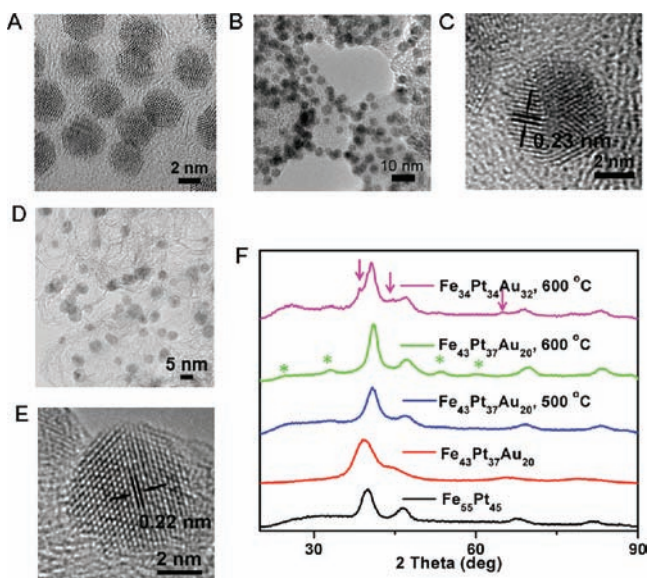
**Figure 1.** TEM images of (A) the as-synthesized 4 nm $Fe_{43}Pt_{37}Au_{20}$ NPs, (B) the $fcc$-$Fe_{43}Pt_{37}Au_{20}$/C NPs, (C) a representative $fcc$-$Fe_{43}Pt_{37}Au_{20}$/C NP, (D) the $fct$-$Fe_{43}Pt_{37}Au_{20}$/C NPs, and (E) a representative $fct$-$Fe_{43}Pt_{37}Au_{20}$/C NP. The as-synthesized NPs were deposited on the amorphous carbon-coated Cu grid, and the other NPs were deposited on the Ketjen carbon support, and they were annealed under 95% Ar + 5% $H_2$ at 400 °C (B,C) and 600 °C (D,E) for 1 h. (F) XRD patterns of the as-synthesized $Fe_{55}Pt_{45}$ NPs, $Fe_{43}Pt_{37}Au_{20}$ NPs and the $Fe_{43}Pt_{37}Au_{20}$ NPs annealed at 500 and 600 °C (stars denote the $fct$-FePt peaks), as well as the $Fe_{34}Pt_{34}Au_{32}$ NPs annealed at 600 °C (arrows denote the Au peaks). The NPs were deposited on the Ketjen carbon support and annealed under 95% Ar + 5% $H_2$ for 1 h.

monodisperse 4 nm FePtAu NPs with Fe/Pt/Au compositions readily controlled by the metal precursor ratios. In this work, the Fe/Pt ratio is kept near 1:1 to facilitate $fcc$–$fct$ phase transformation,[17] while Au is made to have three different percentages so that the Au composition-dependent $fcc$–$fct$ transition and Au-dependent FAOR catalysis can be studied.

High-temperature annealing was applied to remove the surfactants around NPs and to convert the $fcc$-FePtAu to $fct$-FePtAu. To prevent NPs from aggregation under these annealing conditions and to facilitate the catalytic studies, the as-synthesized NPs were deposited on Ketjen carbon (C) support before the annealing (Supporting Information). Figure 1B,C shows the typical TEM and high-resolution (HR) TEM images of the $fcc$-$Fe_{43}Pt_{37}Au_{20}$ NPs annealed under 95% Ar + 5% $H_2$ at 400 °C for 1 h. The $fcc$-$Fe_{43}Pt_{37}Au_{20}$ NPs have an average size of 4 ± 0.2 nm and (111) lattice fringe distance at 0.23 nm. Upon annealing at 600 °C for 1 h, the $fcc$-$Fe_{43}Pt_{37}Au_{20}$ NPs are converted to $fct$-$Fe_{43}Pt_{37}Au_{20}$ NPs, as shown in the TEM and HRTEM images (Figure 1D,E) of the NPs. The NP morphology integrity observed in these TEM images indicates that the FePtAu NPs deposited on the carbon support are well-protected against aggregation/sintering during the high-temperature annealing treatments.

The structure transition of the FePt and FePtAu NPs was monitored by X-ray diffraction (XRD) patterns of the NPs deposited on C (Figure 1F). The as-synthesized $Fe_{43}Pt_{37}Au_{20}$ NPs show a typical $fcc$ pattern with broadened and small angle-shifted peaks compared to the 4 nm $fcc$-$Fe_{55}Pt_{45}$ NPs, suggesting that Au-doping in FePt induces the reduction of crystal coherence length and increase of crystal lattice spacing.

When annealed at 400 and 500 °C for 1 h, the $Fe_{43}Pt_{37}Au_{20}$ NPs remain $fcc$, but at 600 °C for 1 h, the $fcc$-$Fe_{43}Pt_{37}Au_{20}$ is converted to partially ordered $fct$-$Fe_{43}Pt_{37}Au_{20}$. Associated with this structure change, the 4 nm $fct$-$Fe_{43}Pt_{37}Au_{20}$ NPs become ferromagnetic and show a coercivity of ~1000 Oe at room temperature, while the 4 nm $Fe_{55}Pt_{45}$ NPs annealed at the same temperature have a coercivity of only ~300 Oe (Figure S3).[21] This indicates that Au segregation from the FePtAu structure helps to create lattice vacancies within the 4 nm FePtAu structure, promoting Fe/Pt rearrangement. This supports what has been proposed in Au doping effect on FePt structure transformation.[22,23] Our studies further show that the $fct$ structure formation within FePtAu is Au composition-dependent, with Au in 20% (by atomic percentage) range forming better chemical order within the FePt structure. Adding more Au to the FePtAu structure seems to have no benefit for $fcc$–$fct$ transition, as the $Fe_{34}Pt_{34}Au_{32}$ NPs annealed at 600 °C exhibit weaker/broader $fct$ peaks than the $Fe_{43}Pt_{37}Au_{20}$ NPs (Figure 1F).

The carbon-supported $Fe_{43}Pt_{37}Au_{20}$ NPs annealed at 400 and 600 °C respectively were further characterized by atomically resolved aberration-corrected scanning transmission electron microscopy (STEM), STEM-electron energy-loss spectroscopy (STEM-EELS), and STEM-energy dispersive X-ray spectroscopy (STEM-EDS). Figure 2A is the high-angle annular dark
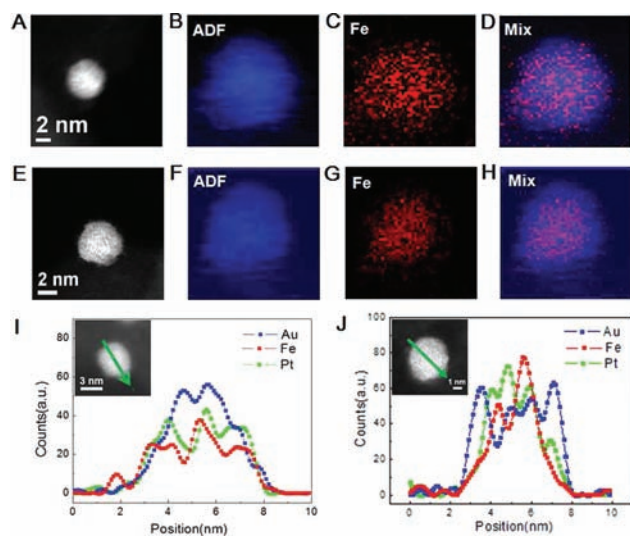


**Figure 2.** (A) STEM imaging and (B−D) simultaneous 2D STEM-EELS mapping from a representative $fcc$-$Fe_{43}Pt_{37}Au_{20}$ NP. (E) STEM imaging and (F−H) simultaneous 2D STEM-EELS mapping from a representative $fct$-$Fe_{43}Pt_{37}Au_{20}$ NP. (I,J) STEM-EDS line scans crossing $fcc$-$Fe_{43}Pt_{37}Au_{20}$ (I) and $fct$-$Fe_{43}Pt_{37}Au_{20}$ (J) NPs. The insets show the NPs scanned.

field (HAADF) image of a representative $fcc$-$Fe_{43}Pt_{37}Au_{20}$ NP, and Figure 2B−D shows the corresponding Fe elemental mapping of this NP using the STEM-EELS method. These analyses indicate that Fe in the $fcc$ structure is uniformly distributed. In contrast, the HAADF image and the corresponding Fe elemental mapping of the $fct$-$Fe_{43}Pt_{37}Au_{20}$ NP (Figure 2E−H) show that Fe is concentrated in the core region and Au/Pt are rich in the shell structure. The STEM-EDS line scans confirm that Au alloys uniformly with Fe and Pt in the $fcc$-$Fe_{43}Pt_{37}Au_{20}$ NPs (Figure 2I), but in the $fct$-$Fe_{43}Pt_{37}Au_{20}$ structure it diffuses out and concentrates around the shell (Figure 2J). Based on the STEM-EELS and STEM-

EDS analyses, the annealing-induced structure change of FePtAu is illustrated in Figure 3. When annealed at 400 °C,
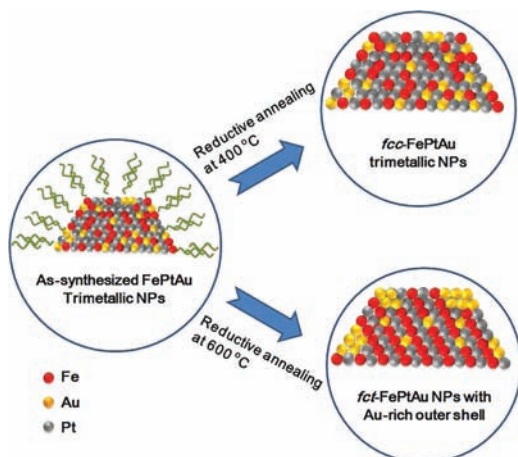


**Figure 3.** Schematic illustration of the structural change of the FePtAu NPs upon annealing. When annealed at 400 °C, the FePtAu NPs have *fcc* structure, but at 600 °C, the *fct*-FePtAu structure is formed, with Au segregating on the NP surface.

the *fcc* structure is better formed in FePtAu NPs. At 600 °C, the *fcc*-FePtAu is converted to *fct*-FePtAu, with Au segregating on the FePt NP surface.[24] Such a unique structure pattern is essential for *fct*-FePtAu NPs to show the enhanced activity and durability for FAOR.

The Au composition effect of the 4 nm *fct*-FePtAu NPs on FAOR was first studied to obtain the optimum Au composition for further catalytic studies. Figure 4A and Figure S4A show the cyclic voltammograms (CVs) of three different kinds of *fct*-FePtAu NPs in $N_2$-saturated 0.5 M $H_2SO_4$ solution. The peaks appearing in the range from −0.25 to 0.15 V are attributed to hydrogen underpotential formation/stripping ($H_{UPD}$) and are used to estimate the electrochemical active surface area of the NPs (Figure S4A).[25] The peaks at 0.3−0.9 V are from metal oxidation/reduction: more Au content in the NP structure leads to stronger Au reduction peaks at 0.80 V (Figure 4A). The electrooxidation activity of these *fct*-FePtAu NPs in 0.5 M $H_2SO_4$ and 0.5 M HCOOH is normalized against NP surface area and is plotted as current density ($J$) vs the applied potentials ($V$) (Figure 4B). For the *fct*-$Fe_{42}Pt_{44}Au_{14}$ NPs, the first current maximum at 0.47 V in the forward scan is due to the direct oxidation of HCOOH to $CO_2$ (dehydrogenation reaction), while the second current maximum at 0.71 V corresponds to oxidation of CO generated from the dehydration reaction of HCOOH.[11] The stability of these *fct*-FePtAu NPs was tested by chronoamperometry, as shown in the $J$ change of FAOR over time ($t$) at 0.2 V (Figure S4B).[26] Among three different kinds of *fct*-FePAu NPs studied, the *fct*-$Fe_{43}Pt_{37}Au_{20}$ NPs have the best long-term stability.

The effect of the structure of the $Fe_{43}Pt_{37}Au_{20}$ NPs on FAOR catalysis was investigated. Figure S5 shows the CVs of the $Fe_{43}Pt_{37}Au_{20}$ NPs annealed at different temperatures. With the increase in annealing temperatures from 400 to 600 °C, the Pt-based reduction peak potentials shift negatively, indicating the better Fe-alloy effect to Pt in *fct*-FePt than in *fcc*-FePt structure. The results of the FAOR catalyzed by the $Fe_{43}Pt_{37}Au_{20}$ NPs annealed at different temperatures are shown in Figure 4C. The *fcc*-$Fe_{43}Pt_{37}Au_{20}$ NPs obtained from 400 °C annealing display an obvious CO oxidation peak at 0.7 V. Increasing the
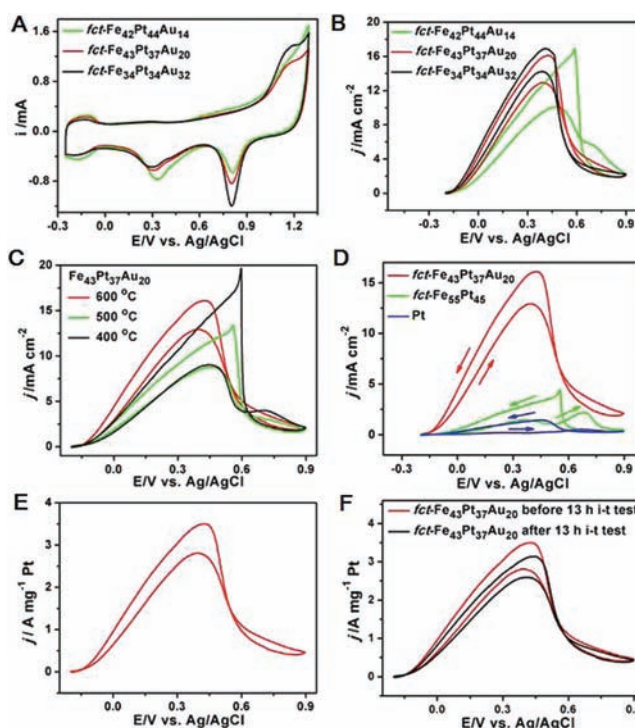


**Figure 4.** (A) CVs and (B) $J−V$ curves of the *fct*-FePtAu NPs with different compositions. (C) $J−V$ curves of the $Fe_{43}Pt_{37}Au_{20}$ NPs annealed at different temperatures. (D) $J−V$ curves of the specific activity of the *fct*-$Fe_{43}Pt_{37}Au_{20}$, *fct*-$Fe_{55}Pt_{45}$ and commercial Pt catalysts. (E) $J−V$ curves of the mass activity of the *fct*-$Fe_{43}Pt_{37}Au_{20}$ NPs. (F) $J−V$ curves of the *fct*-$Fe_{43}Pt_{37}Au_{20}$ NPs before and after a 13 h $I−t$ stability test. The studies were performed in $N_2$-saturated 0.5 M $H_2SO_4$ (for CV curves) and 0.5 M $H_2SO_4$ + 0.5 M HCOOH solutions (for $J−V$ curves).

annealing temperature to 500 °C results in the intensity drop of this oxidation peak. The NPs annealed at 600 °C for 1 h show no CO oxidation peak, suggesting that the segregation of Au on the surface of the *fct*-$Fe_{43}Pt_{37}Au_{20}$ NPs helps CO removal. The FAOR stability of the $Fe_{43}Pt_{37}Au_{20}$ NPs annealed at different temperatures is shown in Figure S6. The $Fe_{43}Pt_{37}Au_{20}$ NPs annealed at 600 °C are more stable for FAOR than any of the other two kinds of NPs treated at 400 and 500 °C, indicating once again that the *fct* structure favors the durability enhancement of FePtAu NPs for FAOR.

The *fct*-$Fe_{43}Pt_{37}Au_{20}$ NPs are much more active and durable catalysts for FAOR than the *fct*-$Fe_{55}Pt_{45}$ NPs and the commercial Pt NPs. Figure S7 and Figure 4D show the comparison of CVs and $J−V$ curves, respectively, for these NPs. As expected, the Pt catalyst has a very strong CO oxidation peak at 0.67 V, whereas the *fct*-$Fe_{55}Pt_{45}$ shows a relatively weak peak at 0.69 V, and the *fct*-$Fe_{43}Pt_{37}Au_{20}$ NPs have no CO oxidation peak. Without the CO-poisoning effect, the *fct*-$Fe_{43}Pt_{37}Au_{20}$ NPs have an onset FAOR potential at −0.2 V, which is 0.12 V lower than that of the commercial Pt (−0.08 V). The mass activity of the 4 nm *fct*-$Fe_{43}Pt_{37}Au_{20}$ NPs reaches 2809.9 mA/mg Pt (Figure 4E), which is the highest among all NP catalysts ever reported. Furthermore, the *fct*-$Fe_{43}Pt_{37}Au_{20}$ NPs are also the most stable NP catalysts for FOAR: their specific activity drops about 50% at the end of a 3 h $J−t$ test (Figure S8). Even after a 13 h $J−t$ test, their mass activity is still at 2600 mA/mg Pt (92.5% of the original value of 2809.9 mA/mg Pt) (Figure 4F). As a comparison, under the same

5062

dx.doi.org/10.1021/ja300708j | *J. Am. Chem. Soc.* 2012, 134, 5060−5063

measurement conditions, the state-of-art PtBi NPs have the mass activity of about 1720 mA/mg Pt and can keep only about 11% of their initial activity at the end of a 3 h *J−t* test.[11]

The *fct*-FePtAu structure with Au segregating on the FePt surface is essential for the NPs to show enhanced activity and durability for FAOR. With the increase of the Au amount to 20% and 32% in the *fct*-Fe$_{43}$Pt$_{37}$Au$_{20}$ and *fct*-Fe$_{34}$Pt$_{34}$Au$_{32}$ NPs, respectively, the CO-related peak in FAOR disappears, indicating that Au on the NP surface promotes the dehydrogenation reaction of HCOOH and inhibits the dehydration reaction that leads to the formation of CO. It seems that Au helps to boost the formation of HCOO$_{ads}$ and its spillover to Pt to facilitate the dehydrogenation pathway.[27] The enhanced stability likely comes from the formation of *fct* structure within *fct*-FePtAu NPs promoted by Au doping and segregation. Without the presence of Au and the formation of *fct* structure, Pt, FePt, and *fcc*-FePtAu NPs are all subject to easy CO poisoning and acid dissolution, exhibiting much lower activity and stability for FAOR than the *fct*-FePtAu NPs.

In summary, this Communication presents a new structure-control strategy to tune and optimize FePtAu NP catalysis for FAOR. These NPs are synthesized by a facile solution-phase process with their compositions controlled by the molar ratios of the metal precursors. The presence of Au in FePt facilitates the FePt structure transformation from *fcc* to *fct* and further promotes the FAOR in the H$_2$SO$_4$ solution. Among all Pt, FePt, and FePtAu NPs tested, the 4 nm *fct*-Fe$_{43}$Pt$_{37}$Au$_{20}$ NPs are the most active and durable catalyst: they have a mass activity of 2809.9 mA/mg Pt and retain 92.5% of this activity after 13 h stability test. The high CO-resistant activity of the *fct*-Fe$_{43}$Pt$_{37}$Au$_{20}$ NPs is attributed to surface segregation of Au from the *fct*-FePt, while the high durability is the result of the formation of the *fct* structure promoted by Au-segregation within the FePtAu NPs. Our preliminary tests show that the *fct*-Fe$_{43}$Pt$_{37}$Au$_{20}$ NPs are also active for catalyzing methanol oxidation reactions with a high CO-tolerance activity (Figure S9). The work demonstrates the great potentials of *fct*-FePtAu NPs as highly efficient catalysts for electrooxidation reactions of organic molecules. More importantly, the structure-control strategy is not limited to FePtAu NPs but can be extended to other M-doped FePtM (M = Cu, Ag, Sb, for example)[18] or Pt- and Pd-based multimetallic NPs, providing a general approach to advanced NP catalysts with simultaneous enhancement in both activity and durability for practical applications.

## ■ ASSOCIATED CONTENT

### Ⓢ Supporting Information

Materials; FePtAu NP synthesis and characterization and their electrochemical measurement; Figures S1−S9. This material is available free of charge via the Internet at http://pubs.acs.org.

## ■ AUTHOR INFORMATION

### Corresponding Author
ssun@brown.edu

### Author Contributions
§These authors contributed equally to this work.

### Notes
The authors declare no competing financial interest.

## ■ ACKNOWLEDGMENTS

## ■ REFERENCES

(1) Tian, N.; Zhou, Z.-Y.; Sun, S.-G.; Ding, Y.; Wang, Z. L. *Science* **2007**, *316*, 732−735.

(2) Lim, B.; Jiang, M.; Camargo, P. H. C.; Cho, E. C.; Tao, J.; Lu, X.; Zhu, Y.; Xia, Y. *Science* **2009**, *324*, 1302−1305.

(3) Gong, K.; Su, D.; Adzic, R. R. *J. Am. Chem. Soc.* **2010**, *132*, 14364−14366.

(4) Wang, C.; Daimon, H.; Onodera, T.; Koda, T.; Sun, S. *Angew. Chem., Int. Ed.* **2008**, *47*, 3588−3591.

(5) Kang, Y.; Murray, C. B. *J. Am. Chem. Soc.* **2010**, *132*, 7568−7569.

(6) Lu, Y.-C.; Xu, Z.; Gasteiger, H. A.; Chen, S.; Hamad-Schifferli, K.; Yang, S.-H. *J. Am. Chem. Soc.* **2010**, *132*, 12170−12171.

(7) Yin, A.-X.; Min, X.-Q.; Zhang, Y.-W.; Yan, C.-H. *J. Am. Chem. Soc.* **2011**, *133*, 3816−3819.

(8) Zhang, H.; Jin, M.; Wang, J.; Li, W.; Camargo, P. H. C.; Kim, M. J.; Yang, D.; Xie, Z.; Xia, Y. *J. Am. Chem. Soc.* **2011**, *133*, 6078−6089.

(9) Zhang, J.; Yang, H.; Fang, J.; Zou, S. *Nano Lett.* **2010**, *10*, 638−644.

(10) Wu, J.; Gross, A.; Yang, H. *Nano Lett.* **2011**, *11*, 798−802.

(11) Ji, X.; Lee, K. T.; Holden, R.; Zhang, L.; Zhang, J.; Botton, G. A.; Couillard, M.; Nazar, L. F. *Nature Chem.* **2010**, *2*, 286−293.

(12) Bing, Y.; Liu, H.; Zhang, L.; Ghosh, D.; Zhang, J. *Chem. Soc. Rev.* **2010**, *39*, 2184−2202.

(13) Cheng, A.; Holt-Hindle, P. *Chem. Rev.* **2010**, *110*, 3767−3804.

(14) Mazumder, V.; Chi, M.; More, K. L.; Sun, S. *J. Am. Chem. Soc.* **2010**, *132*, 7848−7849.

(15) Sasaki, K.; Naohara, H.; Cai, Y.; Choi, Y. M.; Liu, P.; Vukmirovic, M. B.; Wang, J. X.; Adzic, R. R. *Angew. Chem., Int. Ed.* **2010**, *49*, 8602−8607.

(16) Wang, C.; Vliet, D. V. D.; More, K. L.; Zaluzec, N. J.; Peng, S.; Sun, S.; Daimon, H.; Wang, G.; Greeley, J.; Pearson, J.; Paulikas, A. P.; Karapetrov, G.; Strmcnik, D.; Markovic, N. M.; Stamenkovic, V. R. *Nano Lett.* **2011**, *11*, 919−926.

(17) Sun, S. H.; Murray, C. B.; Weller, D.; Folks, L.; Moser, A. *Science* **2000**, *287*, 1989−1992.

(18) Sun, S. H. *Adv. Mater.* **2006**, *18*, 393−403.

(19) Kim, J.; Lee, Y.; Sun, S. *J. Am. Chem. Soc.* **2010**, *132*, 4996−4997.

(20) Yu, X.; Pickup, P. G. *J. Power Sources* **2008**, *182*, 124−132.

(21) Since these NPs are not magnetically saturated, the coercivity values measured from the hysteresis loops are the low-end numbers and are used only to demonstrate the FePt structure conversion. The coercivity values should be larger than the reported once these NPs are magnetically saturated under a stronger magnetic field.

(22) Kinge, S.; Gang, T.; Naber, W. J. M.; Boschker, H.; Rijnders, G.; Reinhoudt, D. N.; van der Wiel, W. G. *Nano Lett.* **2009**, *9*, 3220−3224.

(23) Kang, S.; Jia, A.; Nikles, D. E.; Harrell, J. W. *IEEE Trans. Magn.* **2003**, *39*, 2753−2757.

(24) We should note that to achieve a complete *fcc−fct* transition within 4 nm FePtAu NPs is difficult, as the small NP size tends to restrict the Fe and Pt mobility unless even higher annealing temperate and longer annealing time are applied, which can cause carbon support degradation and FePtAu NP aggregation/sintering.

(25) Snyder, J.; Fujita, T.; Chen, M. W.; Erlebacher, J. *Nat. Mater.* **2010**, *9*, 904−907.

(26) Guo, S.; Zhang, S.; Sun, X.; Sun, S. *J. Am. Chem. Soc.* **2011**, *39*, 15354−15357.

(27) Zhang, S.; Shao, Y.; Yin, G.; Lin, Y. *Angew. Chem., Int. Ed.* **2010**, *49*, 2211−2214.